Photocatalytic Nanorods

Deutsche Ausgabe: DOI: 10.1002/ange.201509115
Internationale Ausgabe: DOI: 10.1002/anie.201509115

TiO_2/Cu_2O Core/Ultrathin Shell Nanorods as Efficient and Stable Photocatalysts for Water Reduction

*Yuanxu Liu, Bingsen Zhang, Liangfeng Luo, Xuanye Chen, Zhonglei Wang, Erlong Wu, Dangsheng Su, and Weixin Huang**

Abstract: *P-type Cu_2O has been long considered as an attractive photocatalyst for photocatalytic water reduction, but few successful examples has been reported. Here, we report the synthesis of TiO_2 (core)/Cu_2O (ultrathin film shell) nanorods by a redox reaction between Cu^{2+} and in-situ generated Ti^{3+} when Cu^{2+}-exchanged H-titanate nanotubes are calcined in air. Owing to the strong TiO_2-Cu_2O interfacial interaction, TiO_2 (core)/Cu_2O (ultrathin film shell) nanorods are highly active and stable in photocatalytic water reduction. The TiO_2 core and Cu_2O ultrathin film shell respectively act as the photosensitizer and cocatalyst, and both the photoexcited electrons in the conduction band and the holes in the valence band of TiO_2 respectively transfer to the conduction band and valence band of the Cu_2O ultrathin film shell. Our results unambiguously show that Cu_2O itself can act as the highly active and stable cocatalyst for photocatalytic water reduction.*

Efficient utilization of solar energy is an attractive and sustainable solution to the energy problem. Hydrogen produced by photocatalytic water splitting over semiconductors by the direct use of sunlight offers a clean and renewable chemical fuel. Since this process is expected to be industrialized at a very large scale, the semiconductor photocatalyst must be low-cost and fabricated from abundant materials using scalable preparation routes. Cuprous oxide (Cu_2O), a p-type oxide with a direct bandgap of 2 eV, has been attracting great interest as the photocatalyst for solar water splitting because of its favorable energy band positions and abundance in the earth, but Cu_2O itself is not stable under solar or photoelectrochemical water splitting conditions.[1–5] Protection of electrodeposited Cu_2O photocathodes with oxide thin overlayers has been examined as an approach for its application in photoelectrochemical water reduction.[6–8] An electrodeposited Cu_2O photocathode protected by nanolayers of aluminum-doped zinc oxide and titanium oxide, and activated by electrodeposited platinum nanoparticles, achieved a Faradaic efficiency close to 100% and remained active after 1 hour of testing,[7] but only 62% activity remained after 10 h of testing.[8] Cu_2O has also been extensively demonstrated as an efficient cocatalyst conjugated with the n-type semiconductor TiO_2 to fabricate the p-n heterojunction in which photoexcited holes transfer from the valence band of TiO_2 to the valence band of Cu_2O and participate in photooxidation reactions therein.[9–13] However, the utilization of Cu_2O itself as active and stable photocatalyst for solar water reduction to hydrogen remains a great challenge and successful examples are few.[14] Herein, we report a highly active and stable TiO_2 (core)/Cu_2O (ultrathin film shell) nanorod photocatalyst in solar water reduction, with methanol as the sacrificial agent, in which the TiO_2 core absorbs the light and both the photoexcited electrons and holes of TiO_2 transfer to the Cu_2O ultrathin film shell to catalyze the water reduction to produce H_2 and the methanol oxidation, respectively.

The TiO_2 (core)/Cu_2O (ultrathin film shell) nanorods were synthesized by a redox reaction between Cu^{2+} and in-situ generated Ti^{3+} (oxygen-vacancy) when Cu^{2+}-exchanged H-titanate nanotubes are calcined in air at 450 °C for 2 h (Scheme 1). The H-titanate exhibits multilayer nanotube structures opening at both ends with interlayer distances of about 0.8 nm, outer diameters less than 12 nm, and lengths from tens up to several hundred nanometers (Supporting Information, Figure S1). The protons in the interlayers of H-titanate nanotubes were demonstrated to facilely exchange with various metal cations,[15,16] and metal-ion-exchanged titanate nanotubes have been used as precursors to prepare TiO_2-based oxide nanocomposites.[17,18] We prepared Cu^{2+}-exchanged H-titanate nanotubes with calculated Cu weight ratios up to 5% (Figure S2), and calcined them in air at 450 °C

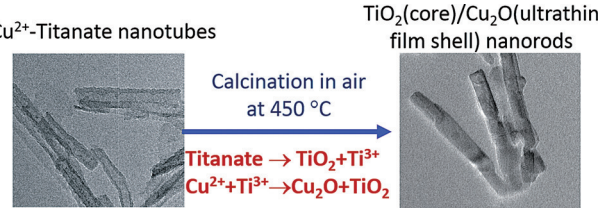

Scheme 1. Illustration of the synthesis of TiO_2 (core)/Cu_2O (ultrathin film shell) nanorods from Cu^{2+}-titanate nanotubes.

[*] Dr. Y. Liu, L. Luo, Z. Wang, E. Wu, Prof. Dr. W. Huang
Hefei National Laboratory for Physical Sciences at the Microscale
CAS Key Laboratory of Materials for Energy Conversion
Department of Chemical Physics
University of Science and Technology of China
Hefei 230026 (P.R. China)
E-mail: huangwx@ustc.edu.cn
Prof. Dr. B. Zhang, Prof. Dr. D. Su
Catalysis and Materials Division
Shenyang National Laboratory for Materials Science
Institute of Metal Research, Chinese Academy of Sciences
Shenyang 110016 (P.R. China)
X. Chen
School of Chemistry and Chemical Engineering
Hefei University of Technology
Hefei 230009 (P.R. China)

Supporting information for this article is available on the WWW under http://dx.doi.org/10.1002/anie.201509115.

for 2 h to acquire the CuO_x/TiO_2 composites. As summarized in Table S1, the actual Cu amount of CuO_x/TiO_2 composites was determined be similar to the calculated values, and their specific surface areas and pore size distributions are similar. Their XRD patterns (Figure S3) only exhibit the diffraction peaks of anatase TiO_2, indicating high dispersions of resultant Cu species.

Anatase TiO_2 nanorods with diameters of 8–15 nm and lengths of several hundred nanometers were acquired when the H-titanate nanotubes were calcined in air at 450 °C for 2 h (Figure S4), agreeing with previous reports.[19] The TEM images show that all CuO_x/TiO_2 composites retain the morphology of nanorods (Figure 1 A1–E1). The diffraction patterns arising from anatase TiO_2 and cubic phase Cu_2O were identified in the ED patterns of CuO_x/TiO_2 composites with Cu loadings up to 1 % wt, while those arising from anatase TiO_2, cubic phase Cu_2O, and monoclinic phase CuO were identified in the 5 % wt-CuO_x/TiO_2 composite. The HRTEM images of 0.05 % wt-CuO_x/TiO_2 (Figure 1 A2 and Figure S5) demonstrate the formation of Cu_2O films with 1–2 nm thicknesses on TiO_2. The thickness of Cu_2O films gradually increases with the copper loading in CuO_x/TiO_2 composites, and in the 1 % wt-CuO_x/TiO_2 composite, the thickest Cu_2O film can reach a thickness of approximately 7 nm (Figure 1 B2–D2 and Figures S6–S8). With the further increase of the copper loading to 5 % wt, (Figure 1 E2 and Figure S9), Cu nanoparticles (NPs) with 2–4 nm sizes were observed on the Cu_2O thin films, but the presence of CuO, instead of Cu, was identified by the ED pattern. This indicates the electron radiation-induced reduction of fine CuO NPs into Cu NPs. These results suggest the formation of TiO_2 (core)/Cu_2O (ultrathin film shell) nanorods for CuO_x/TiO_2 composites up to 1 % wt whose Cu_2O shell thickness increases with the copper loading, and the formation of CuO NP-decorated TiO_2 (core)/Cu_2O (ultrathin film shell) nanorods for the 5 % wt-CuO_x/TiO_2 composite.

Figure 2 A shows the TEM image of a single 1 % wt-CuO_x/TiO_2 nanorod and its HRTEM images of selected regions. Lattice fringes of Cu_2O are clearly visible from the edge to the center throughout the nanorod, while lattice fringes of anatase TiO_2 appear at regions 2–7 nm away from the edge. This suggests the formation of a complete TiO_2 (core)/Cu_2O (ultrathin film shell) nanorod structure. Figure 2 B shows the STEM image and corresponding Ti *K*, Cu *K*, O *K* EDS

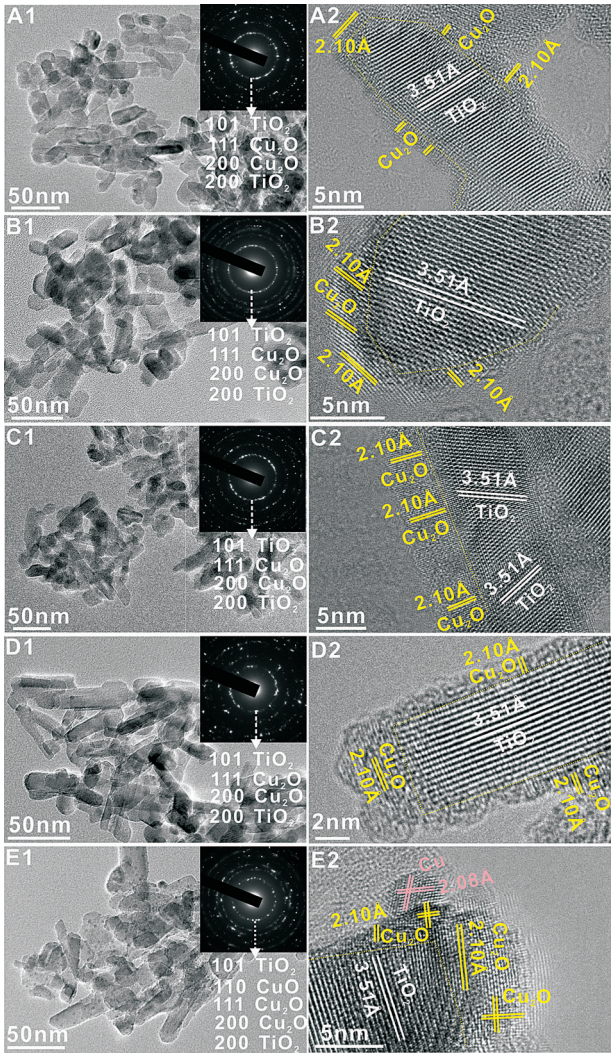

Figure 1. Representative TEM and HRTEM images of (A1 and A2) 0.05 % wt-CuO_x/TiO_2, (B1 and B2) 0.2 % wt-CuO_x/TiO_2, (C1 and C2) 0.5 % wt-CuO_x/TiO_2, (D1 and D2) 1 % wt-CuO_x/TiO_2, and (E1 and E2) 5 % wt-CuO_x/TiO_2 composites. The inset shows the electron diffraction (ED).

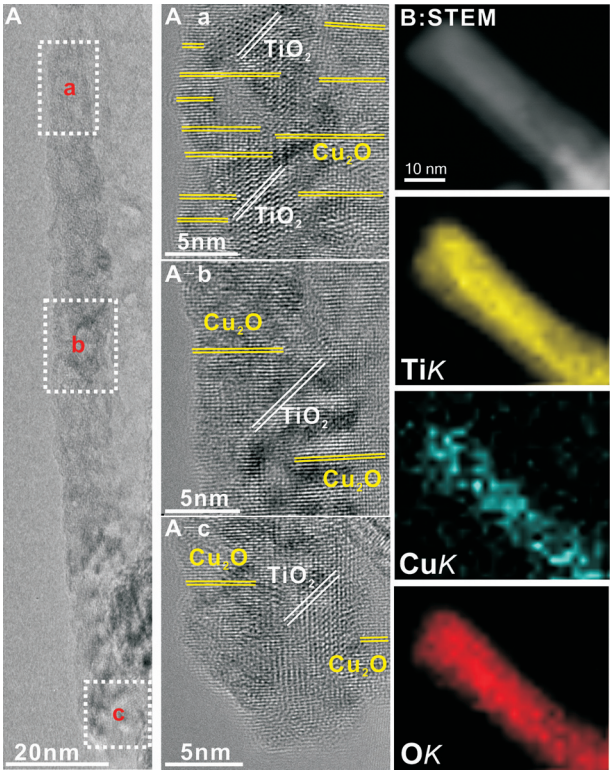

Figure 2. A) TEM image of a single TiO_2 (core)/Cu_2O (ultrathin film shell) nanorod of 1 % wt-CuO_x/TiO_2 composite and the HRTEM images of (A-a) region a, (A-b) region b, and (A-c) region c of the nanorod. B) STEM image and corresponding EDX mapping images of a single TiO_2 (core)/Cu_2O (ultrathin film shell) nanorod of 1 % wt-CuO_x/TiO_2 composite.

mapping images of part of a single 1% wt-CuO_x/TiO_2 nanorod. Elemental mapping images of 1% wt-CuO_x/TiO_2 nanorods at a large scale, including EDS mapping images and energy-filtered TEM images (Supporting Information, Figures S10 and S11). All the mapping images demonstrate the continuous distribution of Cu on the surfaces of the nanorods, further confirming the formation of uniform TiO_2 (core)/Cu_2O (ultrathin film shell) nanorod structure in the 1% wt-CuO_x/TiO_2 composite in which a continuous ultrathin Cu_2O film thinner than 7 nm uniformly covers the TiO_2 nanorod core.

The structural and compositional evolutions of CuO_x/TiO_2 composites were further spectroscopically characterized by XPS and *in-situ* DRIFTS of CO adsorption. The Ti 2p XPS spectra of all CuO_x/TiO_2 composites are similar, exhibiting a single component with its Ti $2p_{3/2}$ binding energy at 458.6 eV (Figure S12), the characteristic of TiO_2.[20] The CuO_x/TiO_2 composites with the Cu loadings up to 1% wt exhibit a single Cu 2p component with its Cu $2p_{3/2}$ binding energy at approximately 932.4 eV whose intensity grows with the Cu loading (Figure 3A). With the further increase of the copper

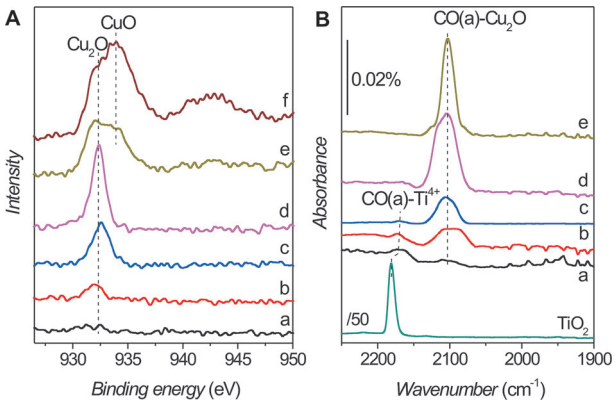

Figure 3. A) Cu $2p_{3/2}$ XPS spectra and B) *in-situ* DRIFTS spectra of CO adsorption of (a) 0.05% wt-CuO_x/TiO_2, (b) 0.2% wt-CuO_x/TiO_2, (c) 0.5% wt-CuO_x/TiO_2, (d) 1% wt-CuO_x/TiO_2, (e) 2% wt-CuO_x/TiO_2, and (f) 5% wt-CuO_x/TiO_2 composites. The *in-situ* DRIFTS spectrum of CO adsorption on bare TiO_2 nanorods is also included as the comparison.

loading above 1% wt, another Cu 2p component appears with its Cu $2p_{3/2}$ binding energy at ca. 933.6 eV and grows at the expense of the Cu 2p component at ca. 932.4 eV. This component is also accompanied by a satellite peak at 942.7 eV. The Cu components with the Cu $2p_{3/2}$ binding energies at ca. 932.4 and 933.6 eV can be assigned to Cu_2O and CuO, respectively.[20] Thus the XPS results demonstrate that only Cu_2O is formed in the surface regions of CuO_x/TiO_2 composites with Cu loadings up to 1% wt-CuO_x/TiO_2, while both Cu_2O and CuO are formed in the surface regions of CuO_x/TiO_2 composites with copper loadings above 1% wt, agreeing with above TEM results.

In the *in-situ* DRIFTS spectra of CO adsorption on bare TiO_2 nanorods at 173 K (Figure 3B), a strong C–O stretch vibration feature was observed at 2181 cm^{-1} and could be assigned to CO(a) at the Ti^{4+} sites.[21] This feature significantly weakens for 0.05% wt-CuO_x/TiO_2 (note that the intensity of *in-situ* DRIFTS spectra of CO adsorption on bare TiO_2 nanorods was divided by 50) and another feature at 2105 cm^{-1} arising from CO(a) at the Cu^+ sites[22] appears. This observation not only confirms the formation of Cu_2O, but also demonstrates that the formed Cu_2O in 0.05% wt-CuO_x/TiO_2 already almost fully covers the TiO_2 nanorods. With the increase of the copper loading, the feature of CO(a) at the Ti^{4+} sites keeps decreasing and vanishes for CuO_x/TiO_2 composites with 1% wt copper loading and above, indicating the gradual formation of continuous Cu_2O film fully covering the TiO_2 nanorods; meanwhile, the feature of CO(a) at the Cu^+ sites keeps increasing until 1% wt-CuO_x/TiO_2 and then slightly decreases for 2% wt-CuO_x/TiO_2. CuO NPs were well established not to adsorb CO,[22] thus the presence of CuO NPs in 2% wt-CuO_x/TiO_2 decreases the amount of accessible Cu_2O for CO adsorption. These CO adsorption results support the formation of a perfect TiO_2 (core)/Cu_2O (ultrathin film shell) nanorod structure for the 1% wt-CuO_x/TiO_2 composite.

The above microscopic and spectroscopic characterization results demonstrate the formation of TiO_2 (core)/Cu_2O (ultrathin film shell) nanorod structures for the CuO_x/TiO_2 composites with Cu loadings up to 1% wt and CuO NP-decorated TiO_2 (core)/Cu_2O (ultrathin film shell) nanorods for the composites with copper loadings above 1% wt. Therefore, redox reactions must occur during the calcination of Cu^{2+}-exchanged H-titanate nanotubes at 450 °C to form Cu_2O. We explored the likely mechanisms with EPR, and the results are shown in Figure 4A. Hydrogen titanate exhibits no

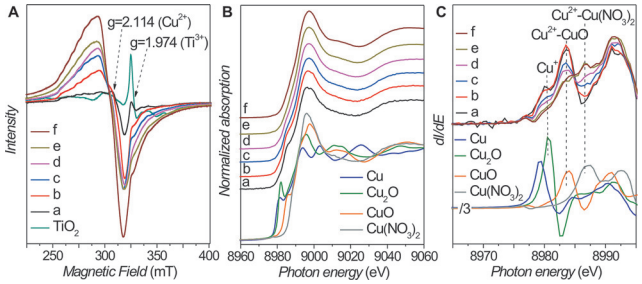

Figure 4. A) EPR spectra, B) Cu K-edge XANES spectra, and C) differentiated Cu K-edge XANES spectra of (a) 0.05% wt-CuO_x/TiO_2, (b) 0.2% wt-CuO_x/TiO_2, (c) 0.5% wt-CuO_x/TiO_2, (d) 1% wt-CuO_x/TiO_2, (e) 2% wt-CuO_x/TiO_2, and (f) 5% wt-CuO_x/TiO_2 composites.

EPR signal, but after its calcination in air at 450 °C for 2 h, the acquired anatase TiO_2 nanorods show a strong EPR signal at $g = 1.974$ that can be assigned to Ti^{3+}.[23] Therefore, Ti^{3+} and accompanying oxygen vacancies are created during the dehydration reaction of hydrogen titanate to produce TiO_2. With the increase of the copper loading in CuO_x/TiO_2 composites up to 1 wt%, the Ti^{3+} EPR signal weakens quickly and disappears at 1% wt-CuO_x/TiO_2. These EPR results suggest that the in-situ generated Ti^{3+} should react with Cu^{2+} to form Cu_2O and Ti^{4+} and be exactly consumed in 1% wt-CuO_x/TiO_2 when Cu^{2+}-exchanged H-titanate nanotubes are calcined in air at 450 °C for 2 h. The produced Cu_2O strongly interacts with and fully wets the simultaneously

resultant TiO_2 nanorods to eventually form the continuous Cu_2O ultrathin film, leading to the TiO_2 (core)/Cu_2O (ultrathin film shell) nanorod structure. The strong Cu_2O–TiO_2 interaction can stabilize Cu_2O not to be oxidized upon calcination in air at 450 °C. However, the stabilization effect depends on the Cu_2O film thickness. In 2 % wt- and 5 % wt-CuO_x/TiO_2 composites, CuO NPs form on the surface and accordingly EPR results show that some Ti^{3+} is not consumed.

An EPR signal at $g = 2.114$ arising from Cu^{2+}[24] was observed to emerge and grow with the copper loading (Figure 4 A), demonstrating the presence of Cu^{2+} in all of the CuO_x/TiO_2 composites. The observation of Cu^{2+} by EPR, but not by XPS, in CuO_x/TiO_2 composites with the Cu loadings up to 1 % wt indicates that the Cu^{2+} should locate in the bulk. In other words, the anatase TiO_2 of CuO_x/TiO_2 composites is doped with Cu^{2+}. The Cu K-edge XANES spectra of CuO_x/TiO_2 composites (Figure 4 B) and the corresponding differential spectra (Figure 4 C) confirm the presence of both Cu_2O and Cu^{2+}, and further demonstrate that the Cu^{2+} dopants in TiO_2 exhibit a CuO-like (fourfold-coordination tetrahedral) local environment at low copper loadings, but both CuO-like and $Cu(NO_3)_2$-like (sixfold coordination octahedra) local environments at large copper loadings. Similar results were also observed in Cu^{2+}-doped TiO_2 samples.[25]

The structures and compositions of 1 % wt-Cu^{2+}-exchanged H-titanate calcined in air at different temperatures for 2 h were also characterized (Figure S13). With the increase of the calcination temperature up to 450 °C, only Cu_2O was observed in the Cu 2p XPS spectra of acquired CuO_x/TiO_2 composites and its intensity keeps increasing whereas the Cu^{2+} EPR signal keep decreasing and no Ti^{3+} EPR signal could be observed. For the CuO_x/TiO_2 composite prepared by the calcination at 550 °C, CuO was observed at the expense of Cu_2O in the Cu 2p XPS spectrum and a tiny Ti^{3+} signal emerges in the corresponding EPR spectrum. Thus the Cu_2O formation is positively correlated to the Ti^{3+} and Cu^{2+} consumptions, further supporting the occurrence of the redox reaction between Cu^{2+} and Ti^{3+} to form Cu_2O and Ti^{4+}. These results also demonstrate that the stabilizing effect of the Cu_2O–TiO_2 interaction on the oxidation-resistance of Cu_2O thin films depends on the calcination temperature.

Figure 5 A shows the photocatalytic activity of TiO_2 and CuO_x/TiO_2 composites in the H_2 production in methanol aqueous reduction under simulated solar light irradiation. Under our photocatalytic reaction conditions, P25 and 1 % wt-Pt/P25 samples exhibit photocatalytic activity of 45.3 and 9950 $\mu mol\,h^{-1}\,g^{-1}$, respectively (Figure S14). The bare anatase TiO_2 nanorods exhibit photocatalytic activity of 83.7 $\mu mol\,h^{-1}\,g^{-1}$. CuO_x/TiO_2 composites are much more photocatalytic active than bare TiO_2, and their H_2 yield increase from 332.7 $\mu mol\,h^{-1}\,g^{-1}$ for 0.05 % wt-CuO_x/TiO_2 to the maximum 1523.2 $\mu mol\,h^{-1}\,g^{-1}$ for 1 % wt-CuO_x/TiO_2, and then decrease to 1193.4 $\mu mol\,h^{-1}\,g^{-1}$ for 2 % wt-CuO_x/TiO_2 and further to 669.7 $\mu mol\,h^{-1}\,g^{-1}$ for 5 % wt-CuO_x/TiO_2. The quantum efficiency of our 1 % wt-CuO_x/TiO_2 composite was measured to be 7.05 % at 365 nm. Although much poorer than 1 % wt-Pt/P25, the H_2 yield and the quantum efficiency of our 1 % wt-CuO_x/TiO_2 composite are among the best data for Cu-containing TiO_2 photocatalysts for the H_2 production in methanol aqueous reduction under simulated solar light irradiation (Table S2). Both the steady-state and the time-resolved photoluminescence spectra (Figure S15) demonstrate that the separation of photon-excited electrons and holes is most efficient within 1 % wt-CuO_x/TiO_2 among all CuO_x/TiO_2 composites, consistent with its highest photocatalytic H_2 production. The UV/Vis DRS spectra (Figure S16) shows that CuO_x/TiO_2 composites absorbs the visible light owing to the presence of Cu_2O, and the absorbance increases with the Cu loading; however, no H_2 production was detected for all of the CuO_x/TiO_2 composites when the UV region below 400 nm of the used simulated solar light was cut off. Therefore, the photocatalytic H_2 production of CuO_x/TiO_2 composites under simulated solar light irradiation should be contributed by the UV light absorbed by TiO_2 but barely by the visible light absorbed by Cu_2O. Within our TiO_2 (core)/Cu_2O (ultrathin film shell) nanorods, the photoexcited electrons in the conduction band of TiO_2 core reasonably could not directly participate in the water reduction owing to the inaccessibility of the TiO_2 core to water. Therefore, in the TiO_2 (core)/Cu_2O (ultrathin film shell) nanorods the TiO_2 core acts as the photosensitizer and the Cu_2O ultrathin film shell acts as the cocatalyst for both the photocatalytic water reduction reaction and the photocatalytic methanol oxidation reaction.

The photocatalytic reaction results suggest that, within our TiO_2 (core)/Cu_2O (ultrathin film shell) nanorods, the holes in the valence band of the TiO_2 core are reasonably

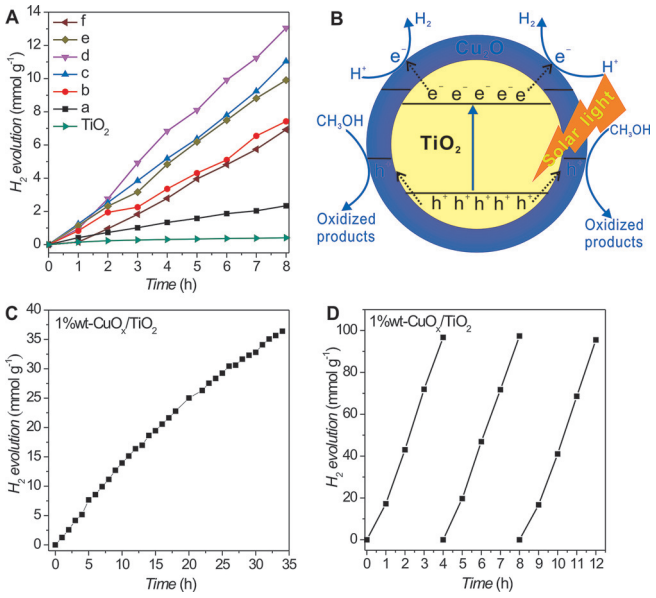

Figure 5. A) Photocatalytic activity for the water reduction under simulated solar light irradiation of (a) 0.05 % wt-CuO_x/TiO_2, (b) 0.2 % wt-CuO_x/TiO_2, (c) 0.5 % wt-CuO_x/TiO_2, (d) 1 % wt-CuO_x/TiO_2, (e) 2 % wt-CuO_x/TiO_2, (f) 5 % wt-CuO_x/TiO_2 composites, and bare TiO_2 nanorods. B) Illustration of the proposed charge transfer mechanism within TiO_2 (core)/Cu_2O (ultrathin film shell) nanorods with buried TiO_2–Cu_2O interfaces. C) Photocatalytic stability of 1 % wt-CuO_x/TiO_2 composite for water reduction under simulated solar light irradiation. D) Photocatalytic activity and stability of 1 % wt-CuO_x/TiO_2 composite for water reduction under UV light irradiation.

transferred to the valence band of the Cu_2O ultrathin film shell with a shallower valence band maximum to catalyze the methanol oxidation, and moreover, the photoexcited electrons in the conduction band of TiO_2 core are also transferred to the conduction band of the Cu_2O ultrathin film shell with a higher conduction band minimum to catalyze the water reduction to produce H_2 (Figure 5B). Such a transfer mechanism of photoexcited electrons at the buried TiO_2–Cu_2O interface of TiO_2 (core)/Cu_2O (ultrathin film shell) nanorod structure does not follow the energy diagram of TiO_2 and Cu_2O (Figure 5B) and the photoexcited electron transfer mechanism always observed in the Cu_2O–TiO_2 p-n heterojunctions with exposed TiO_2–Cu_2O interfaces[9–13] in which the photoexcited electrons in the conduction band of Cu_2O are transferred to the conduction band of TiO_2 with a lower conduction band minimum. The photoinduced charge transfer processes were studied by surface photovoltage (SPV) technique (Figure 6). A SPV response starts to rise when photoinduced excess charge carriers are separated in space.[26]

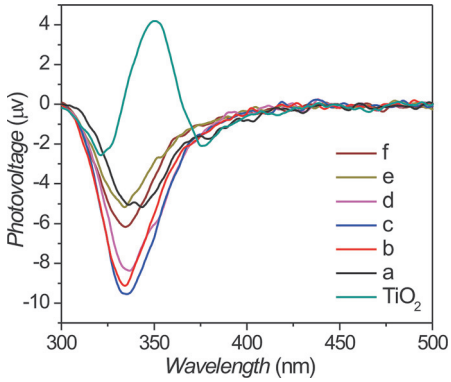

Figure 6. Surface photovoltage spectra of a) 0.05 % wt-CuO_x/TiO_2, b) 0.2 % wt-CuO_x/TiO_2, c) 0.5 % wt-CuO_x/TiO_2, (d) 1 % wt-CuO_x/TiO_2, (e) 2 % wt-CuO_x/TiO_2, f) 5 % wt-CuO_x/TiO_2 composites, and bare TiO_2.

Both bare TiO_2 and CuO_x/TiO_2 composites exhibit measurable surface photovoltages when illuminated by light with wavelengths shorter than 400 nm. This demonstrates that TiO_2 in CuO_x/TiO_2 composites is responsible for the light absorption and charge generation but CuO_x is not. Agreeing with previous results,[27,28] a positive SPV response arises for bare TiO_2, corresponding to the move of the photoexcited holes to the TiO_2 surface driven by the built-in electric field in the surface space charge region with a direction from the bulk towards the surface owing to an upward surface band bending of n-type TiO_2 semiconductor. Negative SPV responses arise for all CuO_x/TiO_2 composites, corresponding to the accumulation of photoexcited electrons on their surfaces that typically occurs for p-type Cu_2O semiconductors exhibiting the built-in electric field in the surface space charge region with a direction from the surface towards the bulk owing to a downward surface band bending.[29,30] These SPV results indicate that all of the CuO_x/TiO_2 composites behave like Cu_2O, consistent with their TiO_2 (core)/Cu_2O (ultrathin film shell) nanorod structures. Moreover, since CuO_x in CuO_x/TiO_2 composites is not responsible for the light absorption and charge generation, the photoexcited electrons accumulated on the surfaces of CuO_x in CuO_x/TiO_2 composites could only be transferred from the TiO_2, directly demonstrating the transfer of photoexcited electrons from the conduction band of the TiO_2 core to the conduction band of the Cu_2O ultrathin film shell.

The photoexcited electrons in the conduction bands of CdS or CdSe cores were previously reported to be transferred to the conduction band of the ZnS shell with a higher conduction band minimum in type I CdS/ZnS or CdSe/ZnS core/shell photocatalysts, and a likely mechanism was proposed to be the electron tunneling of the photoexcited electrons from the core to the shell that typically required a thin shell.[31–33] The Cu_2O shell in our TiO_2 (core)/Cu_2O (ultrathin film shell) nanorods are several nanometers thick, which should allow the electron tunneling process. Therefore, we proposed that the photoexcited electrons in the conduction band of the TiO_2 core at the TiO_2–Cu_2O interface were transferred to the conduction band of Cu_2O ultrathin film shell with a higher conduction band minimum to reduce water into H_2 by the electron tunneling mechanism. Both the electron-participated water reduction reaction in the conduction band of Cu_2O shell and the hole-participated methanol oxidation reaction in the valence band of Cu_2O shell must proceed rapidly to keep such a unique charge transfer mechanism working. Thus, the high photocatalytic activity of our TiO_2 (core)/Cu_2O (ultrathin film shell) nanorod photocatalysts unambiguously indicates the high catalytic activity of Cu_2O in electron-participated water reduction coupled with hole-participated methanol oxidation.

Cu_2O is not stable under standard solar or photoelectrochemical water splitting conditions,[1–5] but our Cu_2O ultrathin film shell on TiO_2 nanorod core turns out to be stable. As shown in Figure 5C, the H_2 production catalyzed by 1 % wt-Cu_2O/TiO_2 keeps stable for 20 h and then slightly decreases, likely owing to the changed H_2 release behaviors with the H_2 partial pressure increasing in the closed system as the photocatalytic reaction continues for a long period. The copper loading of the used 1 % wt-Cu_2O/TiO_2 after the stability test is the same as that of the fresh catalyst, as are its Cu 2p XPS spectrum and HRTEM images (Figure S17). Under UV light irradiation (Figure 5D), the 1 % wt-Cu_2O/TiO_2 composite gives a H_2 yield of 22.3 mmol h^{-1} g^{-1} and remains stable without any loss of Cu during three consecutive cycles of 4 h photocatalytic activity evaluation. The high stability of our Cu_2O ultrathin film shell on a TiO_2 nanorod core in the photocatalytic water reduction reaction can be attributed to the strong TiO_2–Cu_2O interaction at the TiO_2 (core)–Cu_2O (shell) interface formed by the redox reaction between Cu^{2+} and Ti^{3+}. The stabilized Cu_2O ultrathin film shell on a TiO_2 nanorod core is resistant to oxidation at 450 °C, implying that its redox potentials much deviate from those of bulk Cu_2O lying within its bandgap. The stabilizing effect of strong TiO_2–Cu_2O interaction was also demonstrated by the experimental observations that the TiO_2 (core)/Cu_2O (ultrathin film shell) nanorod structure remains intact (Figure S18) even after the 1 % wt-Cu_2O/TiO_2 composite are treated in a 1 mol L^{-1} HNO_3 aqueous solution, although the copper loading decreases from 1.20 % wt to 0.45 % wt.

Thus, we unambiguously demonstrated that Cu_2O itself can act as the highly active and stable cocatalyst for photocatalytic water reduction coupled with photocatalytic methanol oxidation employing a TiO_2 (core)/Cu_2O (ultrathin film shell) nanorod synthesized by a redox reaction between Cu^{2+} and in-situ generated Ti^{3+} during the calcination of Cu^{2+}-exchanged H-titanate nanotubes in air. The strong TiO_2–Cu_2O interfacial interaction not only facilitates the charge transfer process but also stabilizes the Cu_2O ultrathin film. During the photocatalytic water reduction catalyzed by TiO_2 (core)/Cu_2O (ultrathin film shell) nanorods, the TiO_2 core acts as the photosensitizer and the Cu_2O ultrathin film acts as the cocatalyst, and both the photoexcited electrons in the conduction band and the holes in the valence band of TiO_2 core are respectively transferred to the conduction band and the valence band of the Cu_2O ultrathin film shell to efficiently catalyze the water reduction to produce H_2 and the methanol oxidation therein. These results provide a practical strategy for the application of important p-type Cu_2O semiconductors in solar energy utilization.

Acknowledgements

This work was financially supported by National Basic Research Program of China (2013CB933104), National Natural Science Foundation of China (21525313, 21173204, U1332113), Chinese Academy of Sciences (KJZD-EW-M03), MOE Fundamental Research Funds for the Central Universities (WK2060030017, WK2060030022), and Collaborative Innovation Center of Suzhou Nano Science and Technology. We appreciate Prof. Jiaguo Yu (Wuhan University of Technology, China) for his assistance with quantum efficiency measurements, Prof. Tengfeng Xie and Prof. Dejun Wang (Jilin University, China) for their assistance in surface photovoltage (SPV) measurements, and Prof. Xin Xu (University of Science and Technology of China, China) for his assistance in time-resolved photoluminescence spectroscopy measurements.

Keywords: core-shell structures · Cu_2O thin films · interfaces · photocatalysis · redox reaction

How to cite: *Angew. Chem. Int. Ed.* **2015**, *54*, 15260–15265
Angew. Chem. **2015**, *127*, 15475–15480

[1] R. N. Briskman, *Sol. Energy Mater. Sol. Cells* **1992**, *27*, 361–368.
[2] H. Gerischer, *J. Electroanal. Chem. Interfacial Electrochem.* **1977**, *82*, 133–143.
[3] A. V. Walker, J. T. Yates, *J. Phys. Chem. B* **2000**, *104*, 9038–9043.
[4] P. E. de Jongh, D. Vanmaekelbergh, J. J. Kelly, *J. Electrochem. Soc.* **2000**, *147*, 486–489.
[5] S. Kakuta, T. Abe, *Electrochem. Solid-State Lett.* **2009**, *12*, P1–P3.
[6] W. Siripala, A. Ivanovskaya, T. F. Jaramillo, S.-H. Baeck, E. W. McFarland, *Sol. Energy Mater. Sol. Cells* **2003**, *77*, 229–237.
[7] A. Paracchino, V. Laporte, K. Sivula, M. Grätzel, E. Thimsen, *Nat. Mater.* **2011**, *10*, 456–461.
[8] A. Paracchino, N. Mathews, T. Hisatomi, M. Stefik, S. D. Tilley, M. Grätzel, *Energy Environ. Sci.* **2012**, *5*, 8673–8681.
[9] S. Xu, J. Ng, X. Zhang, H. Bai, D. D. Sun, *Int. J. Hydrogen Energy* **2010**, *35*, 5254–5261.
[10] K. Lalitha, G. Sadanandam, V. D. Kumari, M. Subrahmanyam, B. Sreedhar, N. Y. Hebalker, *J. Phys. Chem. C* **2010**, *114*, 22181–22189.
[11] Z. Wang, Y. Liu, D. J. Martin, W. Wang, J. Tang, W. Huang, *Phys. Chem. Chem. Phys.* **2013**, *15*, 14956–14960.
[12] M. Wang, L. Sun, Z. Lin, J. Cai, K. Xie, C. Lin, *Energy Environ. Sci.* **2013**, *6*, 1211–1220.
[13] W.-Y. Cheng, T.-H. Yu, K.-J. Chao, S.-Y. Lu, *ChemCatChem* **2014**, *6*, 293–300.
[14] D. Barreca, P. Fornasiero, A. Gasparotto, V. Gombac, C. Maccato, T. Montini, E. Tondello, *ChemSusChem* **2009**, *2*, 230–233.
[15] X. Sun, Y. Li, *Chem. Eur. J.* **2003**, *9*, 2229–2238.
[16] N. Li, L. Zhang, Y. Chen, M. Fang, J. Zhang, H. Wang, *Adv. Funct. Mater.* **2012**, *22*, 835–841.
[17] J.-C. Xu, M. Lu, X.-Y. Guo, H.-L. Li, *J. Mol. Catal. A* **2005**, *226*, 123–127.
[18] H. Tian, X. L. Zhang, J. Scott, C. Ng, R. Amal, *J. Mater. Chem. A* **2014**, *2*, 6432–6438.
[19] D. V. Bavykin, J. M. Friedrich, F. C. Walsh, *Adv. Mater.* **2006**, *18*, 2807–2824.
[20] J. F. Moulder, W. F. Stickle, P. E. Sobol, K. D. Bomben, *Handbook of X-ray Photoelectron Spectroscopy*, PerkinElmer, Minnesota, **1992**.
[21] W. Su, J. Zhang, Z. Feng, T. Chen, P. Ying, C. Li, *J. Phys. Chem. C* **2008**, *112*, 7710–7716.
[22] A. Martínez-Arias, M. Fernández-García, J. Soria, J. C. Conesa, *J. Catal.* **1999**, *182*, 367–377.
[23] F. Zuo, K. Bozhilov, R. J. Dillon, L. Wang, P. Smith, X. Zhao, C. Bardeen, P. Feng, *Angew. Chem. Int. Ed.* **2012**, *51*, 6223–6226; *Angew. Chem.* **2012**, *124*, 6327–6330.
[24] P. G. Harrison, I. K. Ball, W. Azelee, W. Daniell, D. Goldfarb, *Chem. Mater.* **2000**, *12*, 3715–3725.
[25] J.-N. Nian, S.-A. Chen, C.-C. Tsai, H. Teng, *J. Phys. Chem. B* **2006**, *110*, 25817–25824.
[26] I. Mora-Seró, T. Dittrich, A. Belaidi, G. Garcia-Belmonte, J. Bisquert, *J. Phys. Chem. B* **2005**, *109*, 14932–14938.
[27] V. Duzhko, V. Y. Timoshenko, F. Koch, T. Dittrich, *Phys. Rev. B* **2001**, *64*, 075204.
[28] L. Chen, S. Li, Z. Liu, Y. Lu, D. Wang, Y. Lin, T. Xie, *Phys. Chem. Chem. Phys.* **2013**, *15*, 14262–14269.
[29] D. Gross, I. Mora-Sero, T. Dittrich, A. Belaidi, C. Mauser, A. J. Houtepen, E. Da Coma, A. L. Rogach, J. Feldmann, *J. Am. Chem. Soc.* **2010**, *132*, 5981–5983.
[30] T. Jiang, T. Xie, Y. Zhang, L. Chen, H. Li, D. Wang, *Phys. Chem. Chem. Phys.* **2010**, *12*, 15476–15481.
[31] H. Zhu, N. Song, T. Lian, *J. Am. Chem. Soc.* **2010**, *132*, 15038–15045.
[32] L. Huang, X. Wang, J. Yang, G. Liu, J. Han, C. Li, *J. Phys. Chem. C* **2013**, *117*, 11584–11591.
[33] Y. P. Xie, Z. B. Yu, G. Liu, X. L. Ma, H.-M. Cheng, *Energy Environ. Sci.* **2014**, *7*, 1895–1901.

Received: September 29, 2015
Revised: October 17, 2015
Published online: November 11, 2015

